Manganese-oxidizing photosynthesis before the rise of cyanobacteria

Manganese-oxidizing photosynthesis before the rise of cyanobacteria

Jena E. Johnson[a,1], Samuel M. Webb[b], Katherine Thomas[c], Shuhei Ono[c], Joseph L. Kirschvink[a,d], and Woodward W. Fischer[a]

[a]Division of Geological and Planetary Sciences, California Institute of Technology, Pasadena, CA 91125; [b]Stanford Synchrotron Radiation Lightsource, Stanford University, Menlo Park, CA 94025; [c]Department of Earth, Atmospheric, and Planetary Sciences, Massachusetts Institute of Technology, Cambridge, MA 02139; and [d]Earth-Life Science Institute, Tokyo Institute of Technology, Meguro, Tokyo 152-8550, Japan

Edited* by Andrew H. Knoll, Harvard University, Cambridge, MA, and approved May 22, 2013 (received for review March 25, 2013)

The emergence of oxygen-producing (oxygenic) photosynthesis fundamentally transformed our planet; however, the processes that led to the evolution of biological water splitting have remained largely unknown. To illuminate this history, we examined the behavior of the ancient Mn cycle using newly obtained scientific drill cores through an early Paleoproterozoic succession (2.415 Ga) preserved in South Africa. These strata contain substantial Mn enrichments (up to ∼17 wt %) well before those associated with the rise of oxygen such as the ∼2.2 Ga Kalahari Mn deposit. Using microscale X-ray spectroscopic techniques coupled to optical and electron microscopy and carbon isotope ratios, we demonstrate that the Mn is hosted exclusively in carbonate mineral phases derived from reduction of Mn oxides during diagenesis of primary sediments. Additional observations of independent proxies for O_2—multiple S isotopes (measured by isotope-ratio mass spectrometry and secondary ion mass spectrometry) and redox-sensitive detrital grains—reveal that the original Mn-oxide phases were not produced by reactions with O_2, which points to a different high-potential oxidant. These results show that the oxidative branch of the Mn cycle predates the rise of oxygen, and provide strong support for the hypothesis that the water-oxidizing complex of photosystem II evolved from a former transitional photosystem capable of single-electron oxidation reactions of Mn.

water oxidation | X-ray absorption spectroscopy | Great Oxidation Event | pyrite

The rise of atmospheric oxygen ∼2.4 Ga (1, 2) is the most marked environmental change in Earth history, and this transition ultimately stems from a major biological innovation—the evolution of oxygenic photosynthesis (3, 4). Several biochemical attributes were invented to facilitate this metabolism, including a core photosystem pigment with a higher redox potential than other photosynthetic reaction centers (to enable the oxidation of water) and coupled photosystems. The critical photochemical invention, however, was the water-oxidizing complex (WOC) of photosystem II (PSII)—a cubane cluster of four redox-active Mn atoms and a Ca atom, bound by oxo bridges (5, 6)—which acts as a capacitor to store oxidizing equivalents and link the single-electron photochemistry of the reaction center to the four-electron oxidation of two water molecules to molecular oxygen (7).

Several hypotheses for the origin and evolution of the remarkable water-oxidizing machinery have been proposed. Early ideas suggested a Mn-bearing protein was evolutionarily coopted to become the WOC. In 1970, Olson recognized the need for transitional electron donors with intermediate redox potentials, proposing a series of nitrogen-bearing compounds such as NO and NO_2^- (8). He hypothesized that a Mn(III)-porphyrin cytochrome replaced a Fe-bearing cytochrome as a first step to evolving an Mn-based WOC (8). This idea has become less plausible as the availability of these transitional N compounds is questionable in a preoxygenated world (9), and as our current understanding is that Mn is not bound in a cytochrome but rather a Mn_4CaO_5 cluster (6). Looking to other Mn-bearing proteins as transitional WOCs, Blankenship and Hartman postulated that an Mn-containing catalase transferring electrons from an H_2O_2 donor might have been an intermediate step in the evolution of oxygenic photosynthesis (10). However, there are no significant sequence or structural similarities between the core protein of PSII and Mn catalase, and no evidence for a significant amount of hydrogen peroxide in Archean oceans (10, 11).

A different class of hypotheses suggested that the WOC was derived from the integration of external manganese-oxide phases, building on short-range structural similarities between the WOC and certain tunnel-structured Mn-oxide phases like hollandite (11, 12). This hypothesis, however, is at odds with the general dearth of environmental Mn-oxide phases before the rise of oxygen (13, 14). Furthermore, this process is not recapitulated during formation of the WOC today, which only requires soluble Mn(II) and light (15). During modern assembly of the WOC, no O_2 is evolved, but rather electrons are donated from divalent Mn to the photosystem to arrive at the basal oxidation state (S_0) of the water-oxidizing $Mn(III)_3Mn(IV)$ cluster (4, 7). This mechanism of photoassembly offers a potential clue to the evolution of the WOC.

A Transitional Mn-Oxidizing Photosystem Before Oxygenic Photosynthesis

From an evolutionary perspective, it is notable that modern biological water-splitting begins with Mn oxidation, and this observation forms the basis for a final class of evolutionary scenarios wherein Mn(II) played an important role as an electron donor for photosynthesis before oxygenic photosynthesis. Zubay proposed anoxygenic Fe-based phototrophs developed the capacity for Mn oxidation, which subsequently evolved into a tetramanganese WOC able to store oxidizing equivalents and perform water oxidation (16). Dismukes et al. later hypothesized $Mn(II)(HCO_3)_x$ complexes offered lower potential donors to a transitional photosystem, which then evolved to contain a tetramanganese cluster via a bicarbonate oxidase intermediate that produced O_2 before water splitting (17). Allen and Martin envisioned a protocyanobacterium that started to receive electrons from soluble Mn(II) oxidized by UV radiation (18). These hypotheses differ in their evolutionary mechanics, but all broadly invoke photooxidation of Mn(II)-bearing compounds before the evolution of photochemical water splitting. The high concentrations of Mn(II) in Archean surface seawater (19, 20) would have presented an evolutionary opportunity and electron source for direct Mn(II) oxidation by an early photosystem able to

Author contributions: J.E.J., J.L.K., and W.W.F. designed research; J.E.J., S.M.W., K.T., S.O., and W.W.F. performed research; S.M.W. contributed new reagents/analytic tools; J.E.J., S.M.W., K.T., S.O., and W.W.F. analyzed data; and J.E.J. and W.W.F. wrote the paper.

The authors declare no conflict of interest.

*This Direct Submission article had a prearranged editor.

Freely available online through the PNAS open access option.

[1]To whom correspondence should be addressed. E-mail: jena@caltech.edu.

This article contains supporting information online at www.pnas.org/lookup/suppl/doi:10.1073/pnas.1305530110/-/DCSupplemental.

perform one-electron photochemical reactions. To exploit this resource, a primitive reaction center would have needed to produce a higher potential oxidant to strip electrons from Mn—higher than required for other electron donors but closer to that required for water oxidation. Considering these redox potential constraints, Mn oxidation is an attractive photosynthetic donor on a trajectory to oxidizing water (16–18). An initial manganese-oxidizing photosystem also explains both why the only known biological system that can oxidize water originally procures electrons from Mn and why WOC assembly begins with Mn oxidation. This hypothesis makes a clear prediction: were Mn-based photosynthesis ever realized as a transitional state, it should predate the evolution of oxygenic cyanobacteria. This would leave a distinctive mark in the geological record, with the byproduct of photosynthesis (Mn oxides) forming before the rise of cyanobacteria and in the absence of molecular oxygen.

The timing of cyanobacterial origins remains controversial because of the absence of a robust Archean fossil record. The use of molecular fossils was explored with much apparent potential (21). The 2.7 Ga biomarkers associated with cyanobacteria, 2-methyl hopanoids, suggested the early rise of cyanobacteria, but the syngeneity of these compounds (22) and their connection to cyanobacteria (23, 24) has since been questioned. A separate, widely applied approach to date the evolution of cyanobacteria centers on proxies for their metabolic product: O_2. A variety of geochemical tracers, such as Mo, Re, steranes, and iron speciation, have been used to argue for very low (~ nanomolar) levels of dissolved O_2 implying the evolution of cyanobacteria greatly predates the rise of oxygen (see review by Farquhar et al., 2011, ref. 25). Fundamentally, however, using O_2 as a proxy for cyanobacteria at such low levels is imperfect and will lead to false positives as there are additional sources of O_2 (both biotic and abiotic) that can be important at these concentrations (26–28). Further, many of these elemental proxies have nonunique interpretations and their geochemical cycles are not well understood mechanistically on both short and long timescales (29–31). These proxies can also be impacted by diagenetic and metamorphic processes and studies performed on ancient samples with complex postdepositional histories should be viewed with appropriate caution (29, 32, 33). Sulfur isotope systematics are perhaps the most thoroughly studied, and although the origin of minor isotope mass-anomalous fractionations are not fully understood, the preservation of these effects requires a $pO_2 < 10^{-5.7}$ atm, perhaps closer to 10^{-13} atm (34). Currently, sulfur isotope measurements have constrained the rise of oxygen and minimum age for the origin of cyanobacteria as having occurred between 2.45 and 2.32 Ga (1, 2)—an interval supported by a broad range of geologic evidence (19, 25, 33).

To test these Mn-phototrophy hypotheses, we examined the earliest authigenic Mn deposits paired with several proxies for oxygen to probe the geologic record for evidence of these transitional phototrophs. The behavior of the ancient Mn cycle is useful because it is uniquely sensitive to high-redox-potential oxidants like O_2: unlike other redox proxies, Mn can only be oxidized by molecular oxygen (or O_2-derived species like superoxide and hydrogen peroxide) or a high-potential photosystem (35, 36). It is notable that although Fe was removed from shallow water via oxidation processes in Archean marine environments, the same was not true for Mn (20, 37). In an anoxic Archean world, Mn(II) derived from weathering would have been transported and concentrated in seawater, and, in the absence of high-potential oxidants and because Mn does not readily form sulfides, its primary sink would have been as a trace cation constituent of carbonates. Archean (3.5–2.5 Ga) carbonates consequently have much higher Mn contents, up to 1.3% (38) as opposed to Phanerozoic carbonates averaging 30 ppm (19). Mn can be further enriched in Archean carbonate host rocks by postdepositional carbonate dissolution and oxidation by oxygenated groundwater and hydrothermal fluids after the rise

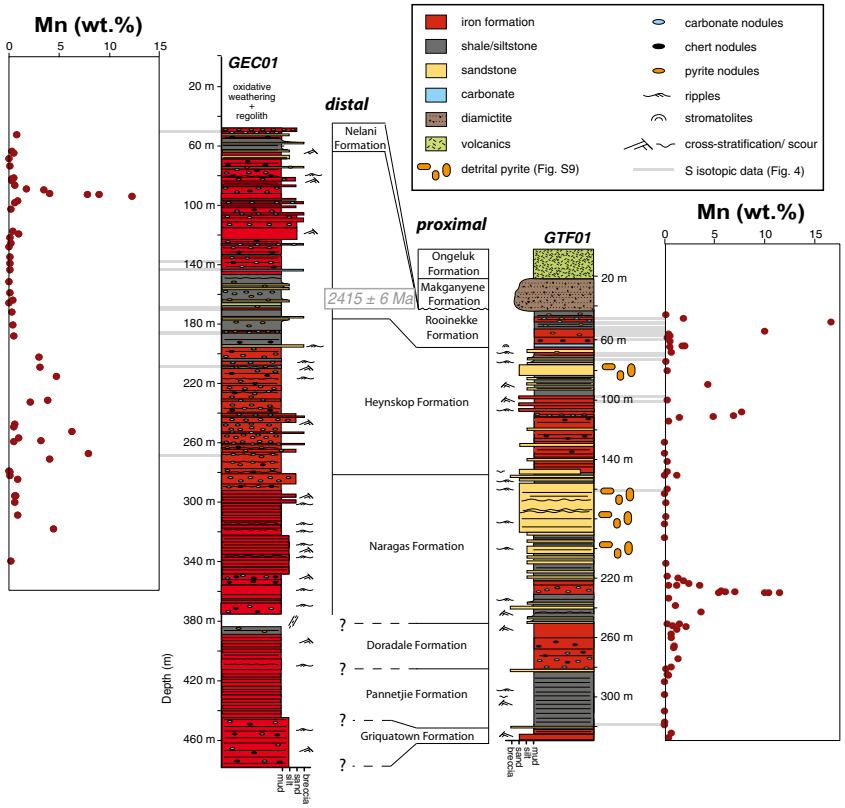

Fig. 1. Stratigraphic columns of drill cores GEC01 and GTF01 showing horizons of Mn enrichments in Agouron drill cores GEC01 and GTF01. Mn abundances were determined by X-ray fluorescence and inductively coupled plasma mass spectrometry. Note the locations of clastic subunits rich in detrital pyrite grains in GTF01 (Fig. S9) and measurements of multiple sulfur isotopes (Fig. 4 and Figs. S7 and S8).

of oxygen (14, 39). Several small Archean-age manganese ore deposits in Brazil, India, and South Africa developed from carbonate protoliths reflect these processes (14). Conversely, chemical precipitates from seawater like iron formation from Archean deposits typically contain Mn <0.5% (40). Oxidation of aqueous Mn(II) to Mn(III/IV) solids is required to concentrate Mn in iron formation (14). Major Paleoproterozoic Mn deposits, including the ~2.22 Ga Kalahari Manganese Field in South Africa, developed in response to the rise in environmental O_2 (41, 42). Here we report the study of a sedimentary succession underlying and substantially older than the Kalahari deposit but also bearing strong authigenic Mn enrichments. We use a suite of microscopic and spectroscopic techniques to determine the petrogenesis of Mn-bearing phases, and then turn to several independent redox-sensitive proxies to ascertain the possible paleoenvironmental role of O_2 in generating these deposits. Examining proxies from a micro- to basin-scale improves the identification of post-depositional alteration, and the use of multiple techniques in the same strata provides an opportunity to address the non-uniqueness common to individual elemental and isotopic proxies.

Results

Manganese Oxidation at 2.415 Ga. Two new scientific drill cores through the 2415 ± 6 Ma Koegas Subgroup (conservatively constrained to be <2.43 Ga and >2.22 Ga, see *SI Text* and ref. 43) were retrieved as a part of the Agouron drilling project in Griqualand West, South Africa (Fig. 1 and Fig. S1). The Koegas Subgroup contains marine shelf and deltaic sediments deposited on the western margin of the Kaapvaal Craton. Observed lithologies include interbedded siliciclastics, iron formation with abundant current and wave ripple cross-stratification, and minor carbonates (43). The two cores are aligned across the strike of the basin and capture proximal (GTF01) and distal (GEC01) paleoenvironments, with a higher proportion of iron formation corresponding to the loss of clastic input basinward (Fig. 1). The inboard sections (GTF01) remain flat lying and are subgreenschist in metamorphic grade (44); whereas, GEC01 is located on the margin of a younger Paleoproterozoic fold-and-thrust belt (Fig. S1), and was more deeply buried to lower greenschist facies with discrete zones of chlorite formation (44). Well captured by the cores, the Koegas strata contain horizons in iron formation with anomalous Mn concentrations (43, 45), ranging from 1% to 16.6% (weight percent) in bulk (Fig. 1, Table S1), which is extremely enriched compared with average Archean iron formation concentrations of <0.5% (40). We observed elevated sedimentary Mn concentrations repeatedly throughout both cores in condensed-sequence stratigraphic intervals (Fig. 1). This illustrates that sedimentary Mn concentrations were high in all environments interpreted as having low relative sedimentation rates (e.g., maximum flooding intervals and delta lobe switches) regardless of position on the shelf or paleowater depth.

The Mn phases responsible for the enrichments in these rocks are very fine-grained and intimately associated with mixed valence iron-bearing minerals, making their analysis by standard methods challenging. Because textural context is critical to understanding the origin of these phases, we used a new set of X-ray absorption spectroscopy techniques that provide insight into redox states and coordination environment of Mn across a large range of length scales. In addition to measuring the X-ray absorption near edge structure (XANES) of the Mn K-edge of bulk powders (Figs. S2 and S3), we used a microprobe technique with 2-μm resolution to obtain XANES spectra on small sample domains and construct microscale redox maps of ultrathin sections (refs. 46 and 47; *SI Text*). We tested these methods on the well-characterized Kalahari Manganese Field of the Hotazel Formation, in which Mn is hosted by two phases, braunite $[Mn(III)_6Mn(II)(SiO_4)O_8]$ and kutnohorite $[(CaMn(II)_{0.7}Mg_{0.3})(CO_3)_2]$ (ref. 48, Figs. S3 and S4). The kutnohorite yields a low $\delta^{13}C$ signature (−8.1‰ to −12.5‰), is found in abundant concretions and laminae, and is interpreted to be secondary and diagenetic in origin from the coupled oxidation of organic carbon and reduction of manganese oxides in sedimentary pore fluids (48, 49), leading to the precipitation of Mn carbonates:

$$2\,MnO_2 + CH_2O + 2\,H^+ \Rightarrow 2\,Mn^{2+} + CO_3^{2-} + 2\,H_2O \qquad [1]$$

$$Mn^{2+} + CO_3^{2-} \Rightarrow MnCO_3 \qquad [2]$$

We acquired XANES spectra of these carbonate concretions and their braunite matrix at a 2-μm resolution (Fig. S3). We then used spectral differences between these end members to distinguish Mn redox states for each pixel and construct a redox map, and no oxides were formed from exposure to modern O_2. A redox map from the Kalahari Mn deposit cleanly differentiates Mn(II) carbonate concretions from the Mn(III+II) braunite matrix (Fig. 2 and Fig. S4).

In contrast to the Kalahari Hotazel Formation, X-ray absorption spectra (XAS) measurements and multiple energy redox maps of 2.415 Ga Mn enrichments throughout both cores, which occur in granular and banded iron formation, reveals that the Mn enrichments are spatially heterogeneous and exclusively

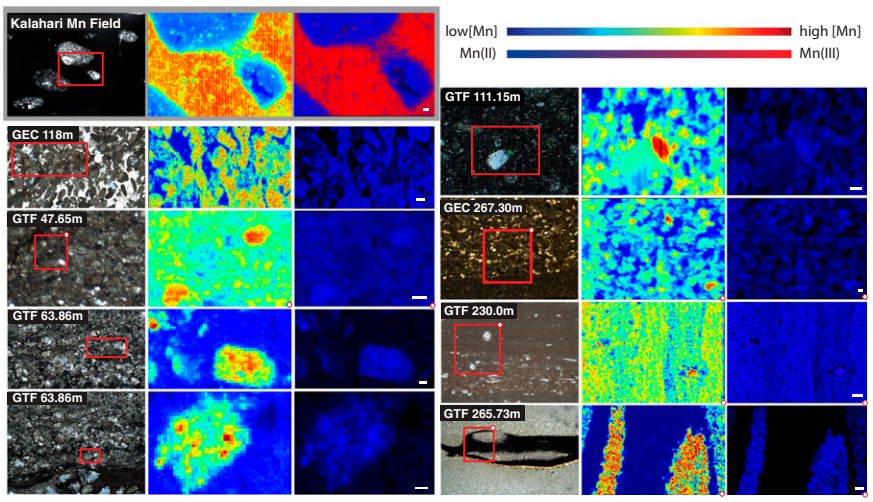

Fig. 2. Transmitted light photomicrographs (*Left*), Mn concentration maps (*Middle*), and Mn redox maps (*Right*). (*Inset*) Red box with small white corner circle highlights the location and orientation of the concentration and redox maps. The X-ray microprobe technique is illustrated on a sample of the ~2.2 Ga Kalahari Manganese Field (gray shading), containing braunite and kutnohorite (Figs. S3 and S4). The remaining samples capture the Mn-rich samples from carbonate-rich granular and banded iron formation of the Rooinekke, Heynskop, and Naragas Formations, and reveal exclusively Mn(II)-bearing phases. Scale bars are 20 μm except GEC 118 m and GTF 230 m, where they are 100 μm. Manganese concentration is in micrograms per square centimeter and on individual scales to highlight within sample heterogeneity: Kalahari (0–1,500); GEC 118 (0–50); GTF 47.65 (0–400); GTF 63.86 (0–200); GTF 111.15 (0–1,000); GEC 267.30 (0–1,000); GTF 230 (0–500); and GTF 265.73 (0–50).

in an Mn(II) valence state (Fig. 2 and Fig. S3*B*). Bulk and point spectra best match kutnohorite and rule out the presence of Mn oxides [Mn(III) or Mn(IV)] at the ∼5% abundance level (at any scale) (Fig. S3). We confirmed the localization and heterogeneity of Mn in carbonate phases by energy-dispersive spectroscopy (Fig. 3 *A* and *B*).

Several independent observations reveal that these Mn carbonates in the Koegas subgroup have a secondary, diagenetic origin from reduction of sedimentary Mn oxide phases, described in Eqs. **1** and **2**. The Mn mineralization is not associated with postdepositional leaching of carbonate beds or more permeable lithologies such as sandstones (Fig. 1). We tested whether later metasomatic fluids (potentially derived from hydrothermal systems in the younger Kalahari Hotazel Formation that occurs ∼150 km to the north; Fig. S1) could have introduced the Mn by measuring concentrations in veins and found they had no Mn enrichments (Fig. S5). Rather, the Mn enrichments are stratigraphically restricted to condensed horizons of iron formation, concentrated in authigenic 10–40-μm Mn-bearing carbonate crystals that display diagenetic textures (Fig. 3 *A* and *B*; Fig. S6). The C isotopic composition of these Mn-carbonate phases is highly variable and strongly ^{13}C depleted from values of seawater dissolved inorganic carbon (Fig. 3*C*; Figs. S7 and S8; Table S2). These observations imply the carbonates were precipitated from pore fluids influenced by the microbial respiration of organic carbon (e.g., Eq. **1**). The Mn and Fe contents of these carbonates, their diagenetic textures, and their carbon isotopic values indicate these secondary carbonates were formed from reduction of Mn and Fe oxides, a process widely recognized from Archean and Paleoproterozoic iron formations (20, 48) and Mn ore deposits (48). Examples of diagenetic Mn-bearing carbonates produced from reduction of Mn oxides are well known from Mesozoic and Neogene deep-sea sediments, driven by reactions with Mn-oxide phases with sedimentary organic matter, and show very similar isotopic characteristics (49, 50). Together these results indicate the sediments accumulated solid Mn-oxide phases, resulting in precursor sediments enriched with Mn oxides at the time of deposition, which were subsequently reduced to Mn carbonate during early diagenesis.

Environmental O_2 Levels Were Very Low During Koegas Deposition. The oxidation of Mn to form these precursor Mn oxides points to the existence of high potential oxidants in the environment before 2.415 Ga. It is notable that although marine paleoenvironments throughout this basin were capable of producing Mn oxides, the sedimentary environment was not able to stabilize them, suggesting the lack of O_2 in this environment. Were O_2 present in surface sediments, then Mn oxides could persist because O_2 is a more favorable electron acceptor (51). To further ascertain whether the Mn oxidant was provided by O_2 or a Mn-oxidizing photosystem, we examined the behavior of several independent redox-sensitive proxies. We investigated whether O_2-sensitive detrital grains were present in intercalated Koegas sandstones and whether early diagenetic pyrite in shale lithologies bears mass-independent S isotope signals.

We observed detrital pyrite grains in subarkosic sandstone beds throughout the GTF01 core (Fig. 1). These redox-sensitive grains offer a simple and straightforward proxy for environmental O_2 because, in the presence of O_2, pyrite is unstable and undergoes rapid oxidative chemical weathering. Consequently, redox-sensitive detrital grains are common in fluvial and nearshore marine sediments before the rise of oxygen (19, 52), and extremely scarce thereafter (19). Physically rounded pyrite grains in these marine sediments (Fig. S9) indicate the lack of O_2 during their weathering, transport, and sedimentation. The detrital origin of these pyrite grains is identified by their rounded, irregular shape; proximity to other dense mineral grains such as zircons and monazites; and in some cases observations of grain-boundary truncations (Fig. S9). We confirmed these grains had a provenance distinct from authigenic pyrite (53) by measuring multiple sulfur isotope ratios from two thin sections using secondary ion mass spectrometry, finding distinct mass-anomalous fractionations (mean $\Delta^{33}S$: −1.12‰; Table S3) that differ from authigenic pyrite with mainly zero or positive $\Delta^{33}S$ (discussed below). Redox-sensitive detrital pyrite is thought to be sensitive to environmental O_2 concentrations of $\sim 10^{-5.7}$ atm (54).

Multiple sulfur isotope ratios ($\delta^{34}S$ and $\Delta^{33}S$) provide another, independent proxy sensitive to very low levels of atmospheric O_2 ($< 10^{-5.7}$ atm; ref. 34), and currently constitute the most established geochemical standard for marking the rise of oxygen (1, 2, 55) [$\delta^{34}S = (([^{34}S/^{32}S_{samp}]/[^{34}S/^{32}S_{std}])-1)1000$; $\delta^{33}S = (([^{33}S/^{32}S_{samp}]/[^{33}S/^{32}S_{std}])-1)1000$; $\Delta^{33}S = 100(\ln(1+(\delta^{33}S/1000)))-0.515(\ln(1+(\delta^{34}S/1000)))$]. In addition to detrital pyrite in the sandstones, Koegas strata contain shale horizons with authigenic sulfide-bearing minerals. However, it is also clear from petrography that these phases record multiple episodes of sulfide mineralization, including euhedral ingrowths and overgrowths, fracture-filling cements, and replacements (Figs. S10 and S11)—requiring careful analysis and interpretation of isotope ratio data. To untangle this history we complimented our bulk SF_6 gas source mass spectrometry analyses with secondary ion mass spectrometry (SIMS) analyses, which enabled us to connect multiple sulfur isotope measurements to texture and insight gained from petrography and cross-cutting relationships (see for example Fig. S12). The SF_6 and SIMS data overlap and record the same systematics (Fig. 4, Figs. S7 and S8, and Table S3). Altogether the multiple sulfur isotope data reveal two discordant isotopic trends. Pyrites with late textures show a $\Delta^{33}S$ near zero and highly variable and

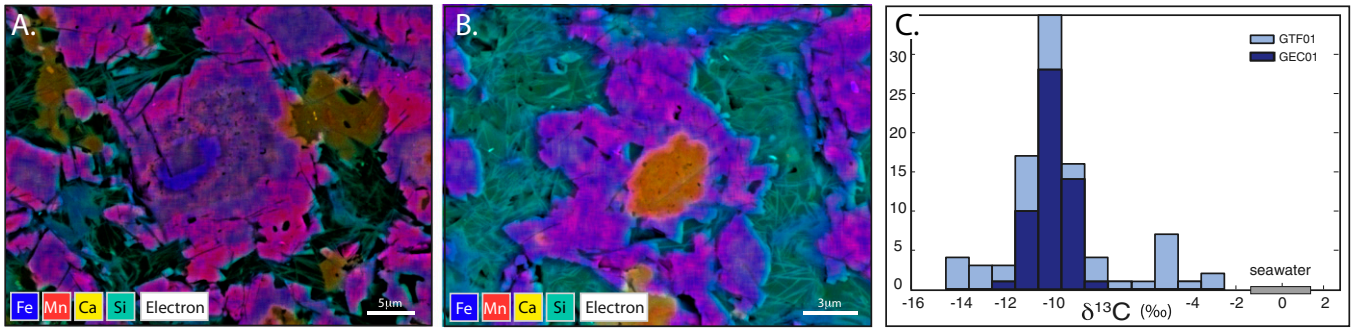

Fig. 3. (*A, B*) Backscatter electron images with overlying electron dispersive spectrometry elemental maps show the variable compositions and diagenetic textures of the Mn-bearing carbonates showing Mn (red), Fe (blue), Ca (yellow), and Si (teal). (*C*) Histogram of $\delta^{13}C$ values (in per mil against Vienna Pee Dee Belemnite) from Mn-rich carbonates in cores. Gray bar denotes estimated (61, 62) seawater dissolved inorganic carbon $\delta^{13}C$.

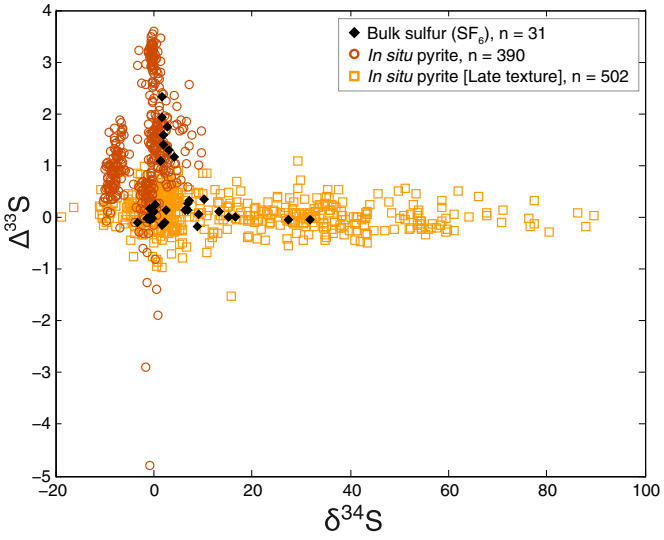

Fig. 4. Multiple sulfur isotope ratio data from GTF01 and GEC01 samples [in per mil against Vienna Canon Diablo Troilite (VCDT)]. SIMS isotope data are further categorized based on petrographic texture (e.g., Figs. S10 and S12). Late pyrites (orange squares) form an array with enriched $\delta^{34}S$ values and $\Delta^{33}S$ near zero and record significant closed system fractionations from late fluids during burial metamorphism and late diagenesis. The 2-σ uncertainties for the SF_6 data are 0.26‰ or better and better than 0.4‰ for SIMS data. The large deviations of $\Delta^{33}S$ from zero for the in situ pyrite (brown circles) is characteristic of Archean- and early Paleoproterozoic–age rocks and indicates an anoxic atmosphere.

positive $\delta^{34}S$ values, whereas pyrites that lack these late textures show $\Delta^{33}S$ values with clear mass anomalous fractionations and muted $\delta^{34}S$ values—two features characteristic of strata deposited before the rise of oxygen (55). These multiple S isotope data imply environmental O_2 concentrations at this time were far less than $10^{-5.7}$ atm (34).

Discussion

The extensive accumulation of manganese-rich deposits *ca.* 2.415 Ga indicates prevalent Mn oxidation, but independent redox-sensitive proxies (detrital pyrite and anomalous multiple S isotope fractionations) suggest environmental O_2 concentrations remained very low. The sedimentary Mn concentrations we observe are too high for abiological mechanisms (*SI Text*) and therefore require a biological oxidation mechanism. This is consistent with idea of transitional Mn-oxidizing phototrophy before the rise of cyanobacteria and oxygenic photosynthesis. However, to examine the possibility that O_2 production by cyanobacteria was responsible for our Mn deposits, we considered scenarios wherein the Mn oxides might have been created by reacting with O_2.

Some have postulated the existence of "oxygen oases" adjacent to cyanobacterial mats before the rise of oxygen, in which oxygen production could exceed the vanishingly low global O_2 average (56). The observations of Mn, redox-sensitive detrital grains, and anomalous multiple sulfur isotope fractionations within Koegas Subgroup facies model do not support the existence of such oases in this sedimentary basin. The Mn enrichments are not uniquely tied to microbial mat lithofacies or a restricted paleoenvironment, but rather are found across the basin, both up- and down- depositional dip, implying a continuity of process over >50 km of the ocean basin that separates our two cores (Fig. S1). This includes deep-water iron formation facies that accumulated chemical sediment from suspension. Moreover, Mn deposits occur in formations spanning the entire Koegas Subgroup, over ∼230 m of stratigraphy in GEC01 and ∼210 m in GTF01. This repeated sequence stratigraphic occurrence indicates Mn deposition across a broad range of space and time, and is not consistent with a transient, restricted mat environment producing O_2. Rather, independent of Mn, all of our observations instead point to its paucity. Shallow-water environments with cross-stratified sandstones have repeated occurrences of redox-sensitive detrital grains in every bed examined throughout the stratigraphy. Shales throughout the stratigraphy have pyrite nodules bearing anomalous sulfur isotope fractionations. These proxies are sensitive to O_2 both locally and globally, and strongly suggest that oxygen oases were not responsible for creating the Mn enrichments in the Koegas Subgroup.

It is also important to consider whether the very low levels of O_2 permissible from the different redox proxies might have been sufficient to oxidize Mn, concentrating oxides in Koegas sediments. It was hypothesized that O_2 cycled as a trace gas before the rise of oxygen (57), and from a thermodynamic perspective, Mn is sensitive to low levels of oxygen (∼10^{-10} atm). However, it is widely recognized that the abiotic kinetics of Mn^{2+} oxidation by O_2 are extremely slow (58). Biological oxidation using O_2 is notably faster (35, 58), but occurs at rates too slow to explain the enrichments observed here. Calculations of Mn oxidation rates at O_2 concentrations of 2.6 nM—the maximum value allowed by multiple sulfur isotope constraints—yield 0.073 g of oxidized Mn per liter per kiloyear, or between 0.02% and 0.2% of the total sediment mass depending on sedimentation rate estimations. These calculations use the maximal biological rates, highest possible dissolved O_2 concentrations, assume conservatively that all Mn oxides reduced were converted to carbonate phases with no return loss to seawater, and still are insufficient to produce these Mn deposits (*SI Text*). For these reasons we do not favor O_2 as the oxidant responsible for creating the sedimentary Mn enrichments we observe. Oxidation rates catalyzed by a photosystem are much faster (59), and consequently we postulate that these Mn deposits were derived from a manganese-based photosynthetic process. Similar to photoferrotrophy proposed for the accumulation of iron in Archean iron formations (60), we interpret the original manganese oxides as products of anoxygenic photobiology, with Mn(II) donating electrons directly to an ancestral reaction center.

The integrated results presented here indicate the oxidative branch of the manganese cycle was operating before 2.415 Ga, but reveal that Mn was not oxidized by O_2. These observations suggest that a transitional photosystem lent the biochemical capability of using Mn as an electron donor, and support a distinct class of hypotheses for the origin of the WOC of PSII that describe single-electron photooxidation reactions involving manganese as an evolutionary intermediate in the development of one of biology's greatest achievements—light-driven water oxidation.

Methods

Bulk Mn abundance was measured using X-ray fluorescence and inductively coupled plasma mass spectrometry. XAS analyses were generated from monolayer powders or ultrathin sections at the Stanford Synchrotron Radiation Lightsource. Thin sections were examined by scanning electron microscope using an energy dispersive spectrometer for elemental mapping. Carbonate $\delta^{13}C$ and $\delta^{18}O$ were measured on a MAT 253 isotope ratio mass spectrometer. Pyrite $\delta^{34}S$ and $\Delta^{33}S$ were measured in bulk on a Thermo 253 dual-inlet mass spectrometer and in situ on a Cameca 7f-GEO. See *SI Text* for additional details on materials and methods.

ACKNOWLEDGMENTS. We thank James Hemp for valuable manuscript feedback; Yunbin Guan and Chi Ma for assistance with SIMS and SEM data collection; Kristin Bergmann for discussions and analytical assistance; and George Rossman, Nic Beukes, Benjamin Kocar, John Eiler, Tim Raub, and John Abelson for helpful discussions and laboratory and field assistance. We thank four anonymous reviewers for valuable insights. Portions of this research were carried out at the Stanford Synchrotron Radiation Lightsource, a Directorate of SLAC National Accelerator Laboratory and an Office of Science User Facility operated for the US Department of Energy Office of Science by Stanford University. Support for this work was provided by the Agouron Institute, National Aeronautics and Space Administration Exobiology (W.W.F.), the David and Lucile Packard Foundation (W.W.F.), and the National Science Foundation Graduate Research Fellowship program (J.E.J.).

1. Bekker A, et al. (2004) Dating the rise of atmospheric oxygen. *Nature* 427(6970): 117–120.
2. Guo Q, et al. (2009) Reconstructing Earth's surface oxidation across the Archean-Proterozoic transition. *Geology* 37(5):399–402.
3. Xiong J, Fischer WM, Inoue K, Nakahara M, Bauer CE (2000) Molecular evidence for the early evolution of photosynthesis. *Science* 289(5485):1724–1730.
4. Williamson A, Conlan B, Hillier W, Wydrzynski T (2011) The evolution of Photosystem II: insights into the past and future. *Photosynth Res* 107(1):71–86.
5. Ferreira KN, Iverson TM, Maghlaoui K, Barber J, Iwata S (2004) Architecture of the photosynthetic oxygen-evolving center. *Science* 303(5665):1831–1838.
6. Umena Y, Kawakami K, Shen J-R, Kamiya N (2011) Crystal structure of oxygen-evolving photosystem II at a resolution of 1.9 Å. *Nature* 473(7345):55–60.
7. McEvoy JP, Brudvig GW (2006) Water-splitting chemistry of photosystem II. *Chem Rev* 106(11):4455–4483.
8. Olson JM (1970) The evolution of photosynthesis. *Science* 168(3930):438–446.
9. Navarro-González R, McKay CP, Mvondo DN (2001) A possible nitrogen crisis for Archaean life due to reduced nitrogen fixation by lightning. *Nature* 412(6842):61–64.
10. Blankenship RE, Hartman H (1998) The origin and evolution of oxygenic photosynthesis. *Trends Biochem Sci* 23(3):94–97.
11. Sauer K, Yachandra VK (2002) A possible evolutionary origin for the Mn4 cluster of the photosynthetic water oxidation complex from natural MnO2 precipitates in the early ocean. *Proc Natl Acad Sci USA* 99(13):8631–8636.
12. Russell M, Allen J, James M-W (2008) Inorganic complexes enabled the onset of life and oxygenic photosynthesis. *Photosynthesis: Energy from the Sun*, eds Allen J, Gantt E, Golbec J, Osmond B (Springer, Dordrecht, The Netherlands), pp 1187–1192.
13. Roy S (1997) Genetic diversity of manganese deposition in the terrestrial geological record. *Manganese Mineralization: Geochemistry and Mineralogy of Terrestrial and Marine Deposits*, eds Nicholson K, Hein JR, Buhn B, Dasgupta S (The Geological Society of London, Bath, UK), pp 5–27.
14. Roy S (2006) Sedimentary manganese metallogenesis in response to the evolution of the Earth system. *Earth Sci Rev* 77(4):273–305.
15. Tamura N, Cheniae G (1987) Photoactivation of the water-oxidizing complex in Photosystem II membranes depleted of Mn and extrinsic proteins. I. Biochemical and kinetic characterization. *Biochim Biophys Acta, Bioenerg* 890(2):179–194.
16. Zubay G (1996) *Origins of Life on the Earth and in the Cosmos* (Academic Press, San Diego), 2nd Ed.
17. Dismukes GC, et al. (2001) The origin of atmospheric oxygen on Earth: The innovation of oxygenic photosynthesis. *Proc Natl Acad Sci USA* 98(5):2170–2175.
18. Allen JF, Martin W (2007) Evolutionary biology: out of thin air. *Nature* 445(7128): 610–612.
19. Holland HD (1984) *The Chemical Evolution of the Atmosphere and Oceans* (Princeton Univ Press, Princeton).
20. Fischer WW, Knoll AH (2009) An iron shuttle for deepwater silica in late Archean and early Paleoproterozoic iron formation. *Geol Soc Am Bull* 121(1/2):222–235.
21. Brocks JJ, Logan GA, Buick R, Summons RE (1999) Archean molecular fossils and the early rise of eukaryotes. *Science* 285(5430):1033–1036.
22. Rasmussen B, Fletcher IR, Brocks JJ, Kilburn MR (2008) Reassessing the first appearance of eukaryotes and cyanobacteria. *Nature* 455(7216):1101–1104.
23. Welander PV, Coleman ML, Sessions AL, Summons RE, Newman DK (2010) Identification of a methylase required for 2-methylhopanoid production and implications for the interpretation of sedimentary hopanes. *Proc Natl Acad Sci USA* 107(19): 8537–8542.
24. Rashby SE, Sessions AL, Summons RE, Newman DK (2007) Biosynthesis of 2-methylbacteriohopanepolyols by an anoxygenic phototroph. *Proc Natl Acad Sci USA* 104(38): 15099–15104.
25. Farquhar J, Zerkle AL, Bekker A (2011) Geological constraints on the origin of oxygenic photosynthesis. *Photosynth Res* 107(1):11–36.
26. Haqq-Misra J, Kasting JF, Lee S (2011) Availability of O(2) and H(2)O(2) on pre-photosynthetic Earth. *Astrobiology* 11(4):293–302.
27. Liang M-C, Hartman H, Kopp RE, Kirschvink JL, Yung YL (2006) Production of hydrogen peroxide in the atmosphere of a Snowball Earth and the origin of oxygenic photosynthesis. *Proc Natl Acad Sci USA* 103(50):18896–18899.
28. Ettwig KF, et al. (2010) Nitrite-driven anaerobic methane oxidation by oxygenic bacteria. *Nature* 464(7288):543–548.
29. Morford JL, Martin WR, Carney CM (2012) Rhenium geochemical cycling: Insights from continental margins. *Chem Geol* 324–325:73–86.
30. Helz GR, Bura-Nakić E, Mikac N, Ciglenečki I (2011) New model for molybdenum behavior in euxinic waters. *Chem Geol* 284(3–4):323–332.
31. Nägler TF, Neubert N, Böttcher ME, Dellwig O, Schnetger B (2011) Molybdenum isotope fractionation in pelagic euxinia: Evidence from the modern Black and Baltic Seas. *Chem Geol* 289(1–2):1–11.
32. Scheiderich K, Zerkle AL, Helz GR, Farquhar J, Walker RJ (2010) Molybdenum isotope, multiple sulfur isotope, and redox-sensitive element behavior in early Pleistocene Mediterranean sapropels. *Chem Geol* 279:134–144.
33. Pufahl PK, Hiatt EE (2012) Oxygenation of the Earth's atmosphere–ocean system: A review of physical and chemical sedimentologic responses. *Mar Pet Geol* 32(3–4):1–20.
34. Pavlov AA, Kasting JF (2002) Mass-independent fractionation of sulfur isotopes in Archean sediments: strong evidence for an anoxic Archean atmosphere. *Astrobiology* 2(1):27–41.
35. Clement BG, Luther GW III, Tebo BM (2009) Rapid, oxygen-dependent microbial Mn(II) oxidation kinetics at sub-micromolar oxygen concentrations in the Black Sea suboxic zone. *Geochim Cosmochim Acta* 73(7):1878–1889.
36. Kopp RE, Kirschvink JL, Hilburn IA, Nash CZ (2005) The Paleoproterozoic snowball Earth: a climate disaster triggered by the evolution of oxygenic photosynthesis. *Proc Natl Acad Sci USA* 102(32):11131–11136.
37. Beukes N, Klein C (1992) Models for iron-formation deposition. *The Proterozoic Biosphere: A Multidisciplinary Study*, eds Schopf JW, Klein C (Cambridge Univ Press), pp 147–156.
38. Komiya T, et al. (2008) Evolution of the composition of seawater through geologic time, and its influence on the evolution of life. *Gondwana Res* 14(1–2):159–174.
39. Varentsov IM (1996) *Manganese Ores of Supergene Zone: Geochemistry of Formation* (Kluwer Academic Publishers, Dordrecht, Netherlands).
40. Klein C (2005) Some Precambrian banded iron-formations (BIFs) from around the world: Their age, geologic setting, mineralogy, metamorphism, geochemistry, and origins. *Am Mineral* 90(10):1473–1499.
41. Kirschvink JL, et al. (2000) Paleoproterozoic snowball earth: Extreme climatic and geochemical global change and its biological consequences. *Proc Natl Acad Sci USA* 97(4):1400–1405.
42. Schissel D, Aro P (1992) The major early Proterozoic sedimentary iron and manganese deposits and their tectonic setting. *Econ Geol* 87(5):1367–1374.
43. Schröder S, Bedorf D, Beukes NJ, Gutzmer J (2011) From BIF to red beds: Sedimentology and sequence stratigraphy of the Paleoproterozoic Koegas Subgroup (South Africa). *Sediment Geol* 236(1–2):25–44.
44. Miyano T, Beukes NJ (1984) Phase relations of stilpnomelane, ferri-annite, and riebeckite in very low-grade metamorphosed iron-formations. *S Afr J Geol* 87(2):111–124.
45. Beukes NJ, Gutzmer J (2008) Origin and paleoenvironmental significance of major iron formations at the Archean-Paleoproterozoic boundary. *Banded Iron Formation-Related High-Grade Ore*, eds Hagemann S, Rosiere C, Gutzmer J, Beukes N (Society of Economic Geologists, Littleton, CO), pp 5–47.
46. Webb SM (2006) SMAK: Sam's Microprobe Analysis Kit (Stanford Synchrotron Radiation Laboratory, Melo Park, CA), v.0.25.
47. Mayhew LE, Webb SM, Templeton AS (2011) Microscale imaging and identification of Fe speciation and distribution during fluid-mineral reactions under highly reducing conditions. *Environ Sci Technol* 45(10):4468–4474.
48. Tsikos H, Beukes NJ, Moore JM, Harris C (2003) Deposition, diagenesis, and secondary enrichment of metals in the Paleoproterozoic Hotazel iron formation, Kalahari Manganese Field, South Africa. *Econ Geol* 98(7):1449–1462.
49. Okita PM, Maynard JB, Spiker EC, Force ER (1988) Isotopic evidence for organic matter oxidation by manganese reduction in the formation of stratiform manganese carbonate ore. *Geochim Cosmochim Acta* 52(11):2679–2685.
50. Matsumoto R (1992) Diagenetic Dolomite, Calcite, Rhodochrosite, Magnesite, and Lansfordite from site 799, Japan Sea - Implications for depositional environments and the diagenesis of organic-rich sediments. *Proceedings of the Ocean Drilling Program, Scientific Results*, eds Pisciotto KA, Ingle JC, Jr., von Breymann MT, Barron J (Ocean Drilling Program, College Station, TX), pp 75–98.
51. Froelich PN, et al. (1979) Early oxidation of organic matter in pelagic sediments of the eastern equatorial Atlantic: Suboxic diagenesis. *Geochim Cosmochim Acta* 43: 1075–1090.
52. Rasmussen B, Buick R (1999) Redox state of the Archean atmosphere: Evidence from detrital heavy minerals in ca. 3250–2750 Ma sandstones from the Pilbara Craton, Australia. *Geology* 27(2):115–118.
53. Hofmann A, Bekker A, Rouxel O, Rumble D, Master S (2009) Multiple sulphur and iron isotope composition of detrital pyrite in Archaean sedimentary rocks: A new tool for provenance analysis. *Earth Planet Sci Lett* 286(3–4):436–445.
54. Anbar AD, et al. (2007) A whiff of oxygen before the great oxidation event? *Science* 317(5846):1903–1906.
55. Farquhar J, Bao H, Thiemens M (2000) Atmospheric influence of Earth's earliest sulfur cycle. *Science* 289(5480):756–759.
56. Kasting JF, Holland HD, Kump LR (1992) Atmospheric evolution: The rise of oxygen. *The Proterozoic Biosphere: A Multidisciplinary Study*, eds Schopf WJ, Klein C (Cambridge Univ Press, Cambridge, UK), pp 1185–1188.
57. Waldbauer JR, Newman DK, Summons RE (2011) Microaerobic steroid biosynthesis and the molecular fossil record of Archean life. *Proc Natl Acad Sci USA* 108(33): 13409–13414.
58. Morgan JJ (2005) Kinetics of reaction between O2 and Mn(II) species in aqueous solutions. *Geochim Cosmochim Acta* 69(1):35–48.
59. Büchel C, et al. (1999) Photoassembly of the manganese cluster and oxygen evolution from monomeric and dimeric CP47 reaction center photosystem II complexes. *Proc Natl Acad Sci USA* 96(25):14288–14293.
60. Konhauser KO, et al. (2002) Could bacteria have formed the Precambrian banded iron formations? *Geology* 30(12):1079–1082.
61. Bekker A, et al. (2001) Chemostratigraphy of the Paleoproterozoic Duitschland Formation, South Africa: Implications for coupled climate change and carbon cycling. *Am J Sci* 301(3):261–285.
62. Fischer WW, et al. (2009) Isotopic constraints on the Late Archean carbon cycle from the Transvaal Supergroup along the western margin of the Kaapvaal Craton, South Africa. *Precambrian Res* 169(1–4):15–27.